SANDIA REPORT
SAND2010-6338
Unlimited Release
Printed September 2010

Injection-Locked Composite Lasers for mm-Wave Modulation: LDRD 117819 Final Report

Anna Tauke-Pedretti, G. Allen Vawter, Weng Chow, Erik Skogen, Mark Overberg, Gregory Peake, Joel Wendt, James Raring, Charles Alford, David Torres, Florante Cajas

Prepared by
Sandia National Laboratories
Albuquerque, New Mexico 87185 and Livermore, California 94550

Sandia National Laboratories is a multi-program laboratory managed and operated by Sandia Corporation, a wholly owned subsidiary of Lockheed Martin Corporation, for the U.S. Department of Energy's National Nuclear Security Administration under contract DE-AC04-94AL85000.

Issued by Sandia National Laboratories, operated for the United States Department of Energy by Sandia Corporation.

Available to DOE and DOE contractors from
U.S. Department of Energy
Office of Scientific and Technical Information
P.O. Box 62
Oak Ridge, TN 37831

Telephone: (865) 576-8401
Facsimile: (865) 576-5728
E-Mail: reports@adonis.osti.gov
Online ordering: http://www.osti.gov/bridge

Available to the public from
U.S. Department of Commerce
National Technical Information Service
5285 Port Royal Rd.
Springfield, VA 22161

Telephone: (800) 553-6847
Facsimile: (703) 605-6900
E-Mail: orders@ntis.fedworld.gov
Online order: http://www.ntis.gov/help/ordermethods.asp?loc=7-4-0#online

SAND2010-6338
Unlimited Release
Printed September 2010

Injection-Locked Composite Lasers for mm-Wave Modulation: LDRD 117819 Final Report

Anna Tauke-Pedretti, G. Allen Vawter, Erik Skogen, Mark Overberg, Gregory Peake, James Raring*
RF/Optoelectronics Department

Weng Chow
Semiconductor Material and Device Sciences Department

Joel Wendt
Photonic Microsystems Technologies Department

Sandia National Laboratories
P.O. Box 5800
Albuquerque, New Mexico 87185-MS1085

Charles Alford
Sandia Staffing Alliance, LLC
Albuquerque, New Mexico 87185

David Torres, Florante Cajas
LMATA Government Services, LLC
Albuquerque, New Mexico 87185

*J. Raring left Sandia employment in January 2008

Abstract

This report summarizes a 3-year LDRD program at Sandia National Laboratories exploring mutual injection locking of composite-cavity lasers for enhanced modulation responses. The program focused on developing a fundamental understanding of the frequency enhancement previously demonstrated for optically injection locked lasers. This was then applied to the development of a theoretical description of strongly coupled laser microsystems. This understanding was validated experimentally with a novel "photonic lab bench on a chip".

ACKNOWLEDGMENTS

The authors would like to acknowledge Zhenshan Yang of Sandia National Laboratories for helpful technical discussions.

CONTENTS

FIGURES

Nomenclature

DOE	Department of Energy
SNL	Sandia National Laboratories
PIC	Photonic Integrated Circuit
EAM	Electro-absorption Modulator
DBR	Distributed Bragg Reflector
MOCVD	Metal-Organic Chemical Vapor Deposition
OSA	Optical Spectrum Analyzer
OIL	Optical Injection Locking

1. INTRODUCTION

The bandwidth of directly modulated lasers is largely defined by the relaxation resonance frequency which is intimately tied to the photon density in the gain region. However, optical injection locking (OIL) has been used extensively in directly modulated lasers to increase the relaxation resonance frequency, reduce nonlinear distortions and reduce chirp [1]. OIL overcomes the dependence of relaxation resonance frequency position on gain section bias current, allowing resonance frequencies as high as 50 GHz [1]. Basically, injecting a laser with a frequency detuned from that laser's optimal frequency enhances the modulation response by roughly the difference of the two frequencies. However, these tabletop experiments were done with multiple discrete devices requiring circulators and isolators, which prevent practical implementation of high performance microsystems. Monolithic integration of the two injection locked lasers has the benefits of reduced coupling losses, increased mechanical robustness, smaller form factor and the compatibility of integration with other elements for the creation of highly functional photonic integrated circuits. Additionally, the fundamental understanding of this frequency enhancement is not well developed. Therefore, in this program we have focused on developing the theoretical basis of injection locking of strongly-coupled laser cavities so as to enable development of high-performance microsystems which exploit injection locking.

We have developed a new theoretical and practical understanding of strongly coupled laser microsystems using combined theoretical work and a novel "photonic lab bench on a chip". Shrinking the lab bench onto a photonic integrated circuit (PIC) (Figure 1) required that two primary obstacles be addressed, removal of the optical isolator and reduction of the time scale of interactions to only a few picoseconds. Accordingly, we developed new theories for frequency- and time- dependent coupled laser systems on the scale of a photonic integrated circuit. We then verified this theory by building a photonic-lab-bench-on-a-chip which microscopically reproduces the laser characteristics and laser-to-laser coupling in order to observe regimes of stable, chaotic, and frequency-enhanced resonant oscillations.

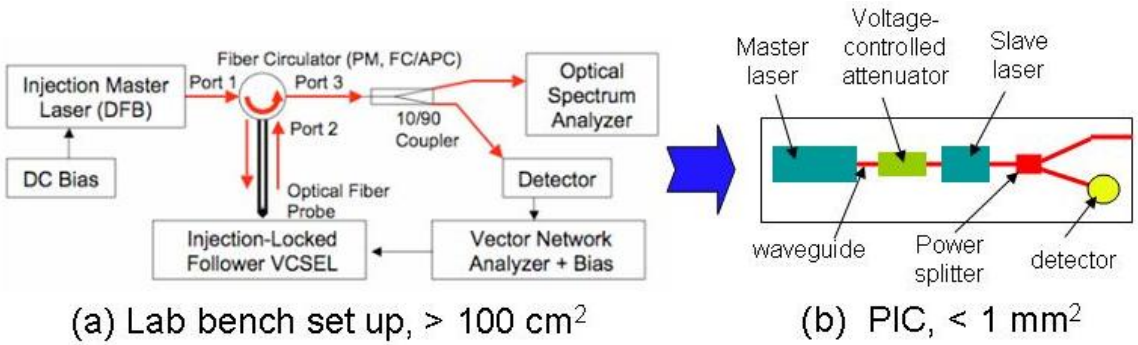

Figure 1: a) large lab bench set-up for injection locking and b) photonic microsystem version.

2. THEORETICAL WORK

This section describes the theoretical work to develop a greater understanding of the bandwidth enhancement in injection locked lasers and the looks at the application of this theory to coupled-cavity devices compatible with integration. The model used in the simulations will be described and the results of these simulations will be presented.

2.1 Description of Model

The models were based on a coupled-cavity device consisting of two laser cavities with DBR mirrors and sharing a central mirror. In a coupled-cavity device, the need to treat the two lasers on equal footing significantly complicates theoretical description. Numerical simulations are also more involved because of a drastic increase in the parameter space controlling dynamical behavior. Therefore, we had to develop an approach for analyzing the consequences of removing the optical isolation between master and slave lasers. Central to the study and new to semiconductor laser modeling is the treatment of the optically-coupled lasers and free space as a combined system. This composite resonator treatment provides a description that is valid for arbitrary coupling (i.e., from complete isolation to totally coupled). Furthermore, it circumvents the long-standing inconsistency involving decoupling the calculations of cavity normal modes and outcoupling losses, which turns out to be important in our problem.

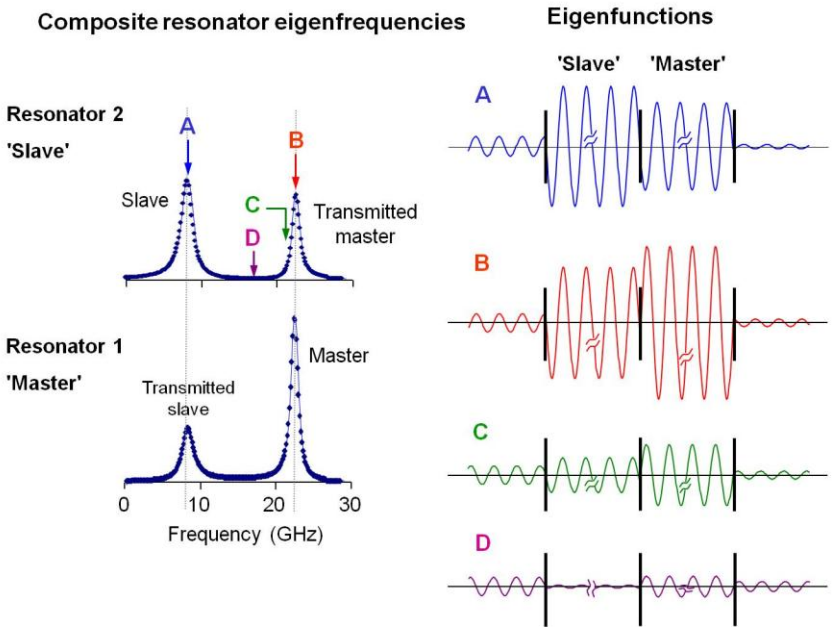

Figure 2: Coupled-laser configuration used in modeling isolator-free injectionlocking. Also plotted are examples of passive-cavity eigenfunctions with frequencies indicated in the spectra showing passive cavity resonances inside Laser 1 (lower spectrum) and Laser 2 (upper spectrum). The points are actual solutions and the curves are extrapolated for the limit L, L'→∞ and $\Gamma_{m,res} = \int_{Z_{res}}^{Z_{res+1}} dz |u_m(z)|^2$.

Since transverse effects are not expected to contribute to the enhancement phenomenon, we consider a 1-dimensional geometry, with the arrangement of the different components of the experimental setup described via the permittivity ε(z), where z is displacement along the laser axis. In principle, one should solve Maxwell's equations using the precise ε(z) describing the spatial variations in permittivity from the different material layers making up the DBRs, quantum wells, spacer layers and waveguides. In practice, such a detailed description is unnecessary and our investigation revealed that dynamical response enhancement depends primarily on the linewidths of the resonators, in addition to detuning and coupling between resonators. Based on this finding, we choose the baseline configuration shown in Figure 2 (right). The DBR sections are replaced by equivalent, infinitely-thin partially-reflecting mirrors that are described by dielectric 'bumps' in the permittivity. Detuning between resonators is determined by difference in round-trip optical path lengths, and cavity lifetimes are determined by the reflectivities of end and shared mirrors, where the latter also controls the optical coupling between resonators. The entire coupled-laser device is embedded in the middle of a very large cavity, approximating free space.[2] End results are extrapolated by taking the limit of an infinitely long large cavity. Writing the laser field as a linear superposition of the eigenmodes of the composite-resonator/free-space system, we derived the following equations of motion for the complex mode amplitudes and carrier densities in both lasers:

$$\frac{dE_m}{dt} = -\sum_{n,res} \gamma_{res}\Gamma_{mn,res}e^{i\omega_{mn}t}E_n + \sum_n g_{mn}e^{i\omega_{mn}t}E_n$$

$$\frac{dN_{res}}{dt} = \frac{J_{res}}{ed} - \gamma N_{res} - \frac{\varepsilon_b}{\hbar\omega}\sum_{m,n}\mathrm{Re}\left(g_{mn}e^{i\omega_{mn}t}E_m^*E_n\right)$$

where

$$g_{mn} = (1-i\alpha)\,A\sum_{res}\Gamma_{mn,res}(N_{res}-N_{tr})$$

$$\Gamma_{mn,res} = \int_{z_{res}}^{z_{res+1}} dz\; u_m(z)\,u_n(z)$$

J_{res} and γ_{res} are the injection current density and distributed optical loss in resonator res, ε_b is the background permittivity inside the lasers, ω is the approximate lasing frequency and γ is an effective carrier loss rate from spontaneous emission and nonradiative recombination. In deriving the equations, we use the rate equation and quasi-equilibrium approximations. Furthermore, we assume a linear carrier density N(z) dependence of material (local) gain and carrier-induced refractive index, $g(z)+ik\delta n(z)=(1-i\alpha)A[N(z)-N_{tr}]$, where α is the linewidth enhancement factor, A is the gain coefficient and N_{tr} is the transparency carrier density. In the limit of operation in a closed, Fabry-Perot resonator, the above equations reduce exactly to the widely-used single-laser rate equations with $\Gamma_{mn,res}\rightarrow\Gamma\delta_{m,n}$, where Γ is the mode confinement factor.

2.2 Results of Models

When attempting to minimize the effects of removing the optical isolator, we search for coupled-laser configurations where the individual lasers exhibit some resemblances of master and slave laser behaviors. Figure 2 (left) shows the passive-cavity resonances in each laser for such a configuration. To produce the desired effect, the resonator optical path lengths are adjusted to give 15-GHz detuning between resonances and the mirror reflectivites are chosen as R_1 = 99%,

$R_2 = 92\%$, and $R_3 = 90\%$. One may reasonably identify Laser 1 as the master laser, based on noting that in the bottom spectra, one of the resonances is a strong narrow peak, resembling a master-laser resonance, and the other is a smaller, broader peak, that may be interpreted as feedback from the slave laser. The top spectra depict a distinctly different situation, with two resonances of roughly equal amplitudes, suggesting a slave laser under strong injection condition. Here, the broad peak is the free-running slave-laser resonance and the narrow peak may be attributed to injection from the master. Comparison of top and bottom spectra shows nonreciprocity in the coupling mirror effective transmission. This asymmetry, achieved without optical isolation, is from resonator linewidth disparity. A second configuration is also model were detuning between resonances is increased to 30 GHz. We kept the end mirror reflectivities at $R_1 = 99\%$, and $R_3 = 90\%$ and decrease the coupling mirror reflectivity to $R_2 = 82\%$ to compensate the reduction in coupling because of increase detuning.

The next step is to explore modulation response enhancement in the above coupled-laser configurations. We apply a 20% sinusoidal modulation to J_2, while operating both lasers above their lasing thresholds. Equations in Section 2.1 are solved numerically for the complex field amplitudes of over 300 eigenmodes describing the combined free-space and composite-resonator system. In the simulations, we use $\alpha_{abs}(\mu_0\varepsilon_b)^{-1/2} = 10^{11}\ s^{-1}$ in free space and $4x10^{11}\ s^{-1}$ inside the lasers, $\gamma = 10^9\ s^{-1}$, $\alpha = 2$, $A = 2 \times 10^{-16}\ cm^2$, $Ntr = 10^{18}\ cm^{-3}$ and lasing wavelength is assumed to be around 1.5 μm. To obtain the modulation response for a given modulation frequency, the time evolution of the total laser field is obtained at each time step. A Fourier transform of the absolute square of the total field over a time interval long compared to the modulation period is then performed to obtain the intensity spectrum. The procedure is repeated until convergence is reached. We define as the modulation response $MR = (B+B')/(2A)$, where B and B' are the spectral amplitudes at $\pm\Omega$, Ω is the modulation frequency, and A is the dc (unmodulated) amplitude.

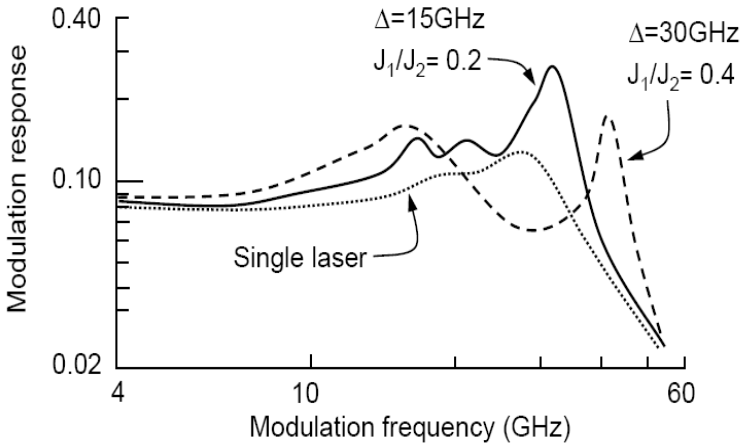

Figure 3: Modulation response vs. modulation frequency for 15GHz detuning, R1=0.99, R2=0.92 and R3=0.90 (solid curve), 30GHz detuning, R1=0.99, R2=0.82 and R3=0.90 (dashed curve) and single laser (dotted curve).

Figure 3 shows examples of results from numerical simulations using the above theory. They illustrate the appreciable sensitivity of modulation response to experimental configuration. We selected coupled-laser configurations where the individual lasers exhibit some resemblances of

master and slave laser behaviors. The curves are obtained by modulating the current to one laser, while operating both lasers above their lasing thresholds. The simulations trace the enhancement of modulation response to the system's ability to generate and support additional frequencies because of spatial hole burning and dynamical bifurcations involving period doubling and perhaps chaos. With spatial hole burning, the fundamental and sideband fields extract gain from different lasers, thus resulting in greater growth of modulation-generated sidebands because of decreased gain competition. Additional frequencies are generated by bifurcations occurring outside the locked region, e.g., period doubling arising from the interaction between nonlinear gain medium and composite-cavity eigenmodes.

2.3 Summary

In summary, coupled-cavity device configurations are found where the results achieved with conventional injection-locked lasers are reproduced. However, eliminating the optical isolator increases significantly the complexity of the problem because master and slave lasers have to be treated on equal footing. A theory capable of treating strongly coupled lasers and providing a rigorous description of outcoupling was developed. The resulting laser model provided understanding of underlying physical mechanisms by tracing dynamical performance improvements to spatial hole burning and dynamical bifurcations arising from the interaction between nonlinear gain medium and coupled-cavity fields. Spatial hole burning allows fundamental and sideband fields to extract gain from different lasers, thus decreasing gain competition that would have inhibited the growth of modulation-generated sidebands. A more through description of the models used can be found in [3-5].

3. EXPERIMENTAL WORK

The new theoretical perspective gained in this program was verified by the performance of coupled-cavity devices designed, fabricated and tested for this project. Two types of PICs were demonstrated. The first is a PIC composed of coupled-cavity DBR lasers where two laser cavities share a central mirror determining the coupling between the laser cavities [6]. Additionally, a coupled-cavity PIC with an EAM between the two laser cavities was explored [7]. This section will described the fabrication of these devices and report the results from devices.

3.1 Device Fabrication

The devices were fabricated in the SNL microfabrication facility. The MOCVD grown epitaxial base structure for this chip consists of seven quantum wells centered in a InGaAsP waveguide layer grown on a conducting sulfur-doped InP substrate. A quantum-well intermixing technique, similar to [8], is used to tailor the quantum well band edge with very low optical reflections allowing the integration of different functionalities on the chip. The chips consist of active optical regions for the laser gain section, intermediate regions with a slightly blue-shifted bandedge, ~50 nm, for the EAMs, and passive regions with a fully blue-shifted bandedge, ~100 nm, for waveguide, phase and grating sections. The DBR mirrors are defined with e-beam lithography and dry etched into the semiconductor. Following the definition of the mirror gratings, there is a single planar MOCVD regrowth of the InP p-cladding and p-doped InGaAs contact layer. Topside n-contacts, designed for high-speed probing, are formed using dry etching, metal deposition and annealing. Bis-benzocyclobutene (BCB) was used as a low-k dielectric under the p-contact pads to reduce the capacitance and isolate the n-metal and p-metal. A proton implant was used to isolate the p-contacts of the laser sections and EAM. A single layer AR coating was used to suppress facet back reflections. The devices were cleaved and soldered to copper submounts. The DC contacts were wirebonded to an AlN standoff and the high-speed laser gain sections and EAMs were directly probed using a ground-signal-ground high-speed probe for testing. A micrograph of a fabricated and mounted chip is in Figure 4.

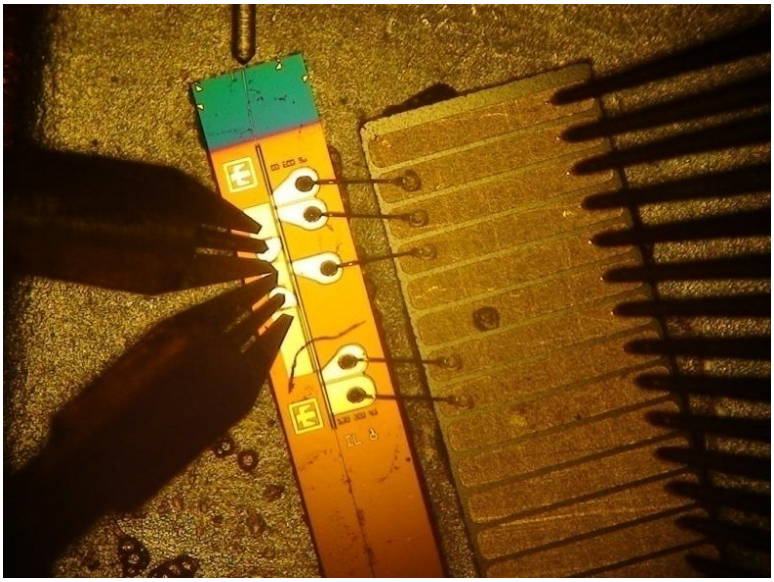

Figure 4 : Optical micrograph of the coupled cavity PIC during testing.

3.2 Coupled-Cavity Mutually Injection-Locked Lasers

The coupled-cavity device consists of two DBR lasers sharing a center mirror (Figure 5). Although there is not a clearly defined master and slave laser due to coupling between the lasers, for reference purposes the laser nearest the output will be referred to as the slave and the back laser will be referred to as the master. The slave laser consists of a 58 µm front mirror, a 50 µm phase section, a 200 µm gain section and a 45 µm rear mirror. The rear mirror of the slave laser is shared between the two lasers and also acts as the front mirror for the master laser. The master laser consists of the shared mirror, a 500 µm gain section, a 50 µm phase section and a 150 µm rear mirror. The DBR mirrors were designed for effective power reflectivities of 90%, 45% and 99% for the slave front mirror, shared mirror and master rear mirror respectively. The ridge waveguide is 4 µm wide with a curved and flared output to reduce back reflections and improve coupling efficiency.

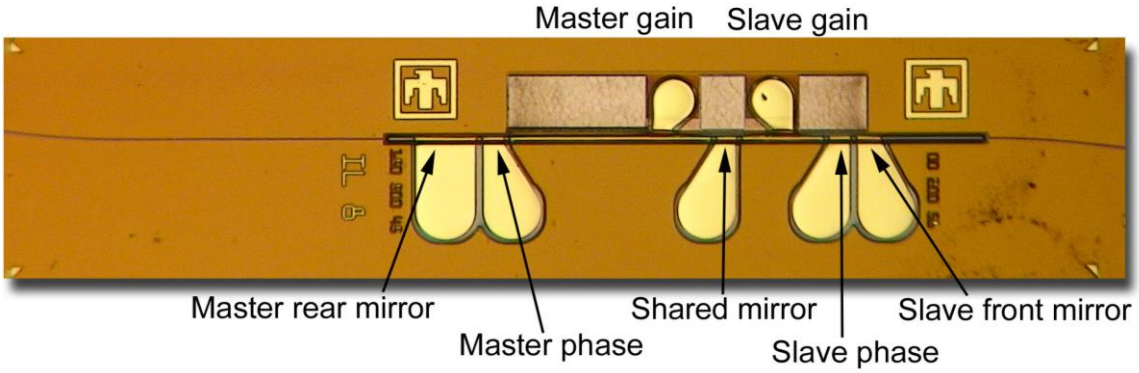

Figure 5 : Optical micrograph of the coupled cavity PIC die.

3.2.1 External Injection Measurements

The coupled-cavity devices were first characterized with an external laser to verify the well documented injection locking behavior between two lasers separated with an optical isolator. The frequency response of the slave laser under external injection was taken for a number of different injected powers (Figure 6). Light from a tunable external cavity laser was coupled into the slave laser cavity. A circulator was used to separate the laser output light from the injected light. The output of the modulated slave laser was input into a photodiode and then port 2 of a network analyzer. The master laser gain section was reverse biased to -4 V rendering it effectively an absorber. The level of injected power into the laser cavity was measured by reverse biasing the slave laser gain section to -4 V and recording the measured photocurrent. Injection locking operation was verified by observation that the slave's lasing wavelength is identical to master's wavelength in an OSA. In this case the PIC slave laser is acting as a true slave laser and the external cavity laser is the injection locking master laser. There is a 0.1 nm detuning between the free running wavelength of the slave laser and the injected external laser as determined by measurements on an OSA. The resonance peak moves out in frequency and is dampened in amplitude with increasing injection power. This is in agreement with other reported devices and theory [9].

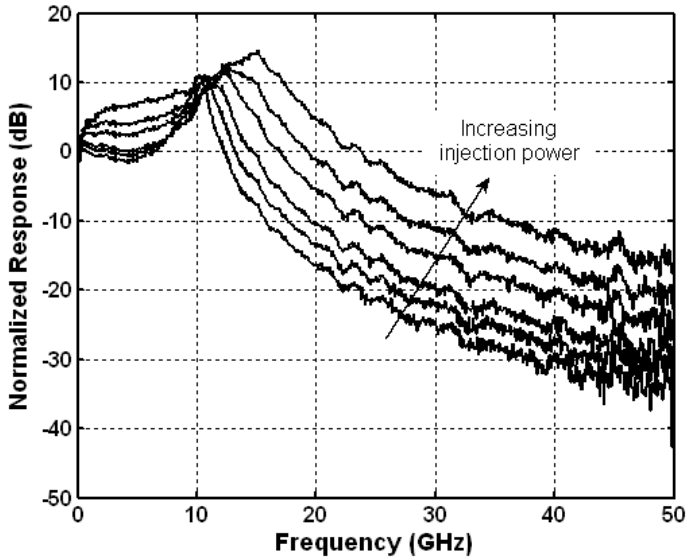

Figure 6: Slave laser under external injection for injected powers of 0.91 mW, 1.14 mW, 1.44 mW, 1.79 mW, 2.26 mW, and 2.84 mW. Master laser gain section is reverse biased. (I_{gain}=31 mA, $I_{phase} = I_{front\ mirror} = I_{rear\ mirror}$ = 0 mA, $\lambda_{injected}$ = 1556.36 nm)

3.2.2 Coupled-Cavity Mutual Injection Locking Measurements

The coupled nature of the two lasers on the chip prevents the lasers from sharing a free running wavelength. Therefore, single frequency operation indicates the lasers are operating in the mutual injection locked regime. Due to the lack of optical isolation, there are three active cavities in the PIC that create a complex cavity mode spacing. The relative cavity lengths and mode spacing of the lasers were tuned by applying current to the laser phase and mirror sections to achieve mutual injection locking over a wide range of master gain biases. The resulting side

mode suppression ratio (SMSR) for the PIC was greater than 30 dB for all measurements as shown in Figure 7.

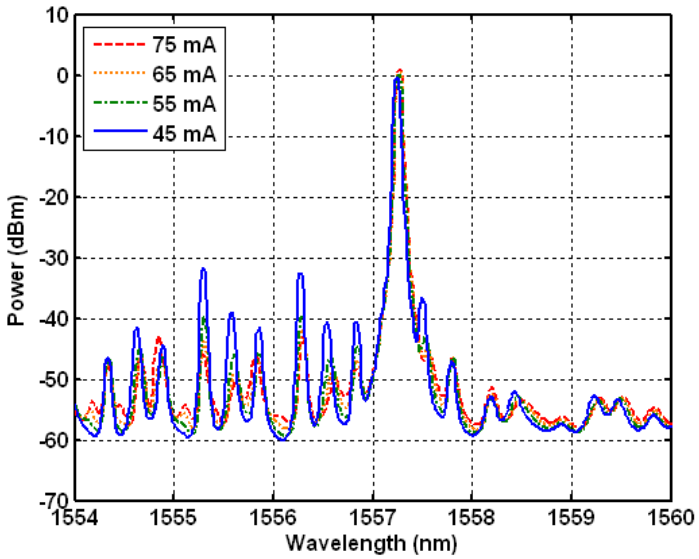

Figure 7: Spectra of the coupled cavity device for varying master laser gain currents. ($I_{slave\ gain}$ = 31 mA, $I_{slave\ phase}$ = 9.8 mA, $I_{slave\ front\ mirror}$=1 mA, $I_{shared\ mirror}$=$I_{master\ phase}$=$I_{master\ rear\ mirror}$=0 mA)

The small signal frequency response of the PIC was characterized using a 50 GHz network analyzer. The output of the network analyzer was used to directly modulate the gain section of the slave laser. Meanwhile, the gain section of the master laser was biased at a constant current level. The light output of the device was coupled into a lensed fiber, detected by a high speed photodiode and the resulting electrical signal was directed to port 2 of the network analyzer. Measurements were taken for varying levels of master laser gain current. The resulting frequency response measurements are shown in Figure 8. The free running frequency response of the slave laser is taken with the master laser gain section biased at 0 mA and shows a resonance frequency of 3 GHz. This resonance moves out to beyond 30 GHz when the lasers are mutually injection locked. The resonance frequency continues to increase and dampen as the current is increased in the master laser gain section, due to the increasing the photon density in the modulated slave laser.

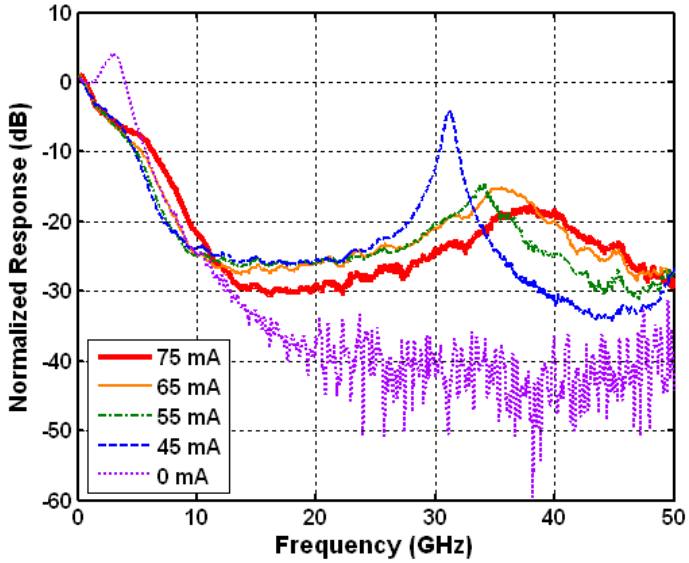

Figure 8: Small signal frequency response of the coupled cavity device for varying master laser gain currents. ($I_{slave\ gain}$ = 31 mA, $I_{slave\ phase}$ = 9.8 mA, $I_{slave\ front\ mirror}$=1 mA, $I_{shared\ mirror}$=$I_{master\ phase}$=$I_{master\ rear\ mirror}$=0 mA)

The small signal frequency response was also taken with varying levels of the slave phase current (Figure 9). This changes the effective cavity length of the slave laser and as a result the detuning between the free running wavelengths of the master and slave is altered. The detuning is measured as the difference between the peak wavelength and the nearest cavity mode seen in the spectra. The resonance frequency directly correlates to the difference between the lasing wavelength and the nearest cavity mode seen in the optical spectra. The detuning decreases with increased phase current, moving the frequency resonance with it.

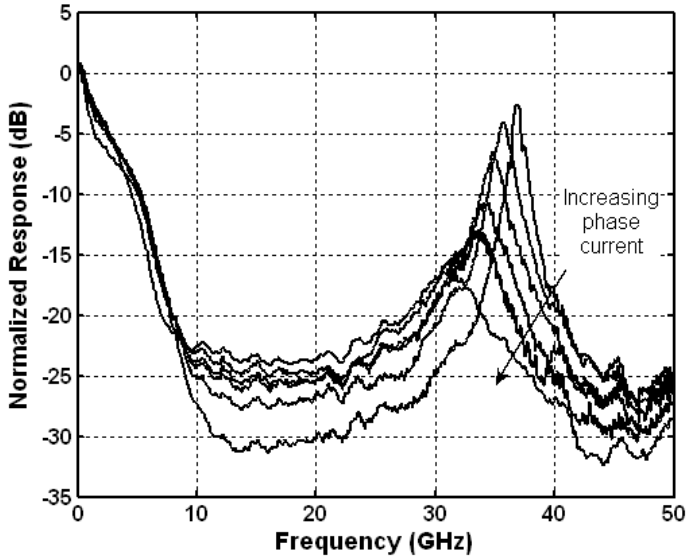

Figure 9: Small signal frequency response of the coupled cavity device for phase section currents of 14 mA, 10 mA, 9 mA, 8 mA, 7 mA, and 6 mA.. ($I_{slave\ gain}$ = 31 mA, $I_{master\ gain}$ = 55 mA, $I_{slave\ phase}$ = 9.8 mA, $I_{slave\ front\ mirror}$=1 mA, $I_{shared\ mirror}$=$I_{master\ phase}$=$I_{master\ rear\ mirror}$=0 mA)

3.2.3 Coupled-Cavity DBR Summary

We have demonstrated an increase of the relaxation resonance frequency in a PIC composed of two coupled DBR lasers. The relaxation resonance frequency moved from 3 GHz for a single directly modulated laser to beyond 30 GHz with the mutual injection locking of the lasers. The observed injection locking dynamics for the coupled-cavity device is consistent with tabletop systems employing discrete lasers and circulators. This compact chip is compatible with further integration enabling highly functional PICs to take advantage of the benefits of OIL.

3.3 Mutually Injection-Locked Lasers Integrated with an EAM

Recent research in optical injection locking (OIL) of directly modulated lasers has shown increases in the relaxation resonance frequency, reductions of nonlinear distortions and reductions in chirp [1,10]. However, in OIL lasers, increases in the relaxation resonance frequency do not always translate into increased bandwidth due to a low frequency pole from the laser carrier dynamics limiting the bandwidth before the relaxation resonance frequency. It was recently reported that the injection of externally modulated master laser light can overcome this limitation and does not exhibit the severe response dips seen in directly modulated lasers with OIL [11]. While these are promising results, the size, complexity, and sensitivities of the discrete component configuration stands in the way of practical implementation. Monolithic integration of the two lasers and modulator on a single compact chip has the benefits of reduced coupling losses, increased mechanical robustness, smaller form factor and the compatibility of integration with other elements for the creation of highly functional photonic integrated circuits. Such a chip would not be able to utilize optical isolators resulting in the intimate coupling of the laser cavities. Therefore, we have modified our coupled-cavity DBR design to incorporate an EAM. This compact photonic integrated circuit (PIC) incorporates two distributed Bragg reflector (DBR) lasers and an electro-absorption modulator (EAM).

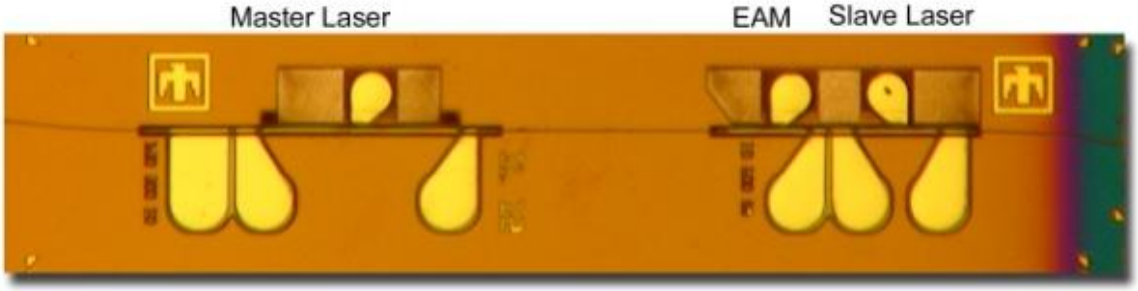

Figure 10: Optical micrograph of the PIC consisting of (from left to right) the master DBR laser, EAM, slave DBR laser and output waveguide.

3.3.1 Design

The PIC consisting of two DBR lasers and a 200 μm long EAM positioned between the lasers was fabricated on an InP-based integration platform. An optical micrograph of the device is

shown in Figure 10. Although there is not a clearly defined master and slave laser due to coupling between the lasers, for reference purposes the laser farthest from the front facet will be referred to as the master laser and the laser closest to the facet is referred to as the slave laser. A 4 µm wide ridge waveguide guides the light and connects all the circuit elements. This ridge is curved and flared at the output to increase coupling efficiency and reduce reflections. Devices of two different coupling strengths were characterized. This coupling strength is defined by front mirror of the master laser and the rear mirror of the slave laser.

3.3.2 71% Mirror Reflectivity Design

The PIC design with weaker coupling between the lasers has mirrors designed for 99%, 71%, 71% and 90% reflectivities for the master rear mirror, master front mirror, slave rear mirror and slave front mirror respectively. Physically this means the master laser consists of a 150 µm long rear mirror, 50 µm long phase section, 500 µm long gain section and 38 µm long front mirror. The slave laser consists of a 38 µm long rear mirror, 50 µm long phase section, 200 µm long gain section and 58 µm long front mirror.

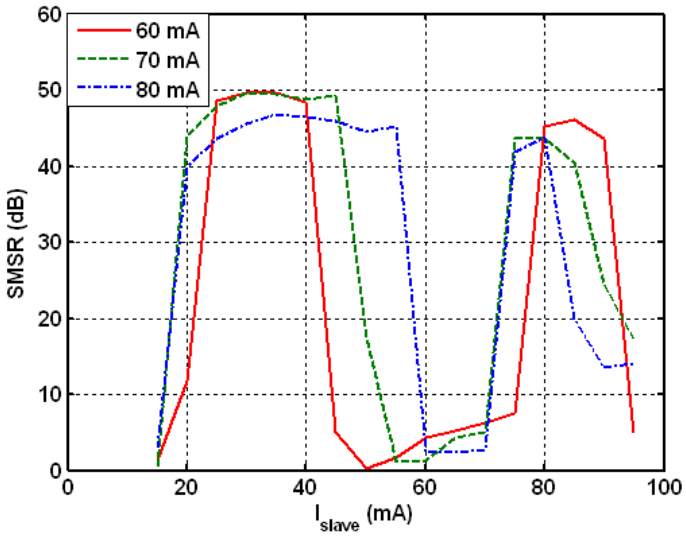

Figure 11: SMSR vs. slave laser gain current for varying master laser gain currents. (V_{EAM} = -1.5 V).

Similar to the coupled-cavity laser, the coupling of the two lasers on the chip prevents the lasers from sharing a free running wavelength. Therefore, single-frequency operation indicates the lasers are operating in the mutual injection locked regime. Due to the lack of optical isolation, there are five active cavities in the PIC which creates a complex cavity mode structure. The relative cavity lengths and mode spacing of the lasers can be tuned by applying current to the laser phase and mirror sections to achieve mutual injection locking over a wide range of master gain biases. The injection locked bands of the PIC can be traced out by plotting the side-mode suppression ratio (SMSR). A high (>30 dB) SMSR indicates the lasers operating at a single frequency and thus are injection locked. The SMSR of the PIC as a function of the slave laser electrical bias is plotted in Figure 11 for three different master laser gain biases. This plot shows two separate lock-bands. In the first band where the slave gain bias is low, the master laser is controlling the slave laser and defining the output wavelength. As the master gain bias increases this lock-band widens due to the corresponding increase in power injected into the slave laser cavity. In the second lock-band where the slave gain bias current is high, the slave laser is

controlling the master laser and the output modes. This lock-band narrows with increasing master laser bias current due to a reduction in the relative power ratio. The locking behavior seen in this integrated device agrees with the behavior seen in tabletop experiments utilizing isolators [9].

The small signal frequency response of the PIC was characterized using a 50 GHz network analyzer. The output of the network analyzer was connected to the EAM. A 50 Ω load resistor was connected in parallel with the EAM for impedance matching. Meanwhile, the gain sections of the two lasers were biased at a constant current level. The optical output signal from the PIC was coupled into a lensed fiber and collected by a high speed photodiode. The generated electrical signal was applied to the input port of the network analyzer. For all the measurements, the lasers were biased in the first mutual injection locking regime, which was confirmed with measurements of the optical spectra showing SMSR greater than 30 dB.
The EAM frequency response is taken using a separate chip consisting of a DBR laser integrated with an EAM. The bandwidth of the EAM is 10 GHz and limited by the resistance and capacitance of the device and load resistor (Figure 12).

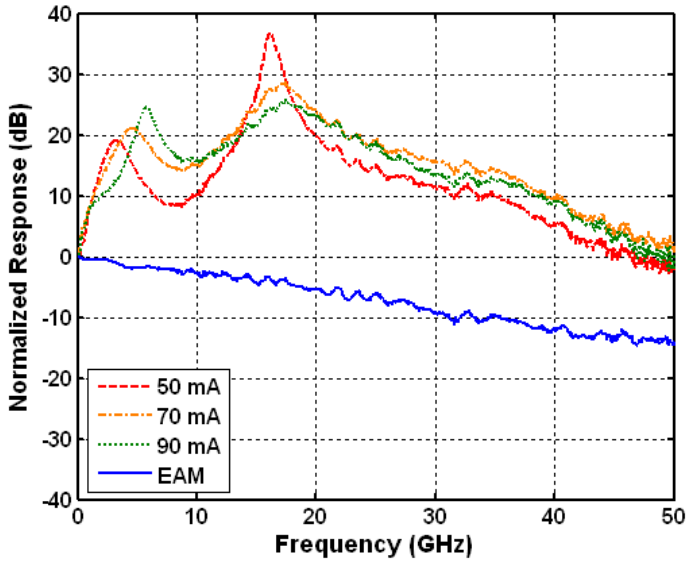

Figure 12: The small-signal frequency response of the coupled cavity device for varying master laser gain current ($I_{slave\ gain}$ = 31 mA, V_{EAM} = -2V) and of the laser-EAM (V_{EAM} = -2V).

Measurements were taken for varying levels of master laser gain current. The resulting frequency response measurements are shown in Figure 3.10. There are two distinct resonances in the optical response. It has been shown that the location of resonance peaks in optical injection locked responses closely correlate with the detuning between the lasing wavelength and the cavity modes of the free running laser [12]. The complex cavity of the PIC presented here creates many closely spaced modes allowing the frequency modulation to correspond to the detuning for multiple modes in the 50 GHz frequency scan. If the frequency response was extended to higher frequencies additional resonances would be expected, similar to the discrete-laser case. The changes in the gain current affect both the positions and amplitudes of the resonances due to changes in the photon density and cavity spacing. Similar to a single directly modulated laser, increases in the internal photon density result in the damping of

relaxation resonance. The modal cavity spacing changes with injected gain current because the injected carriers change the refractive index and effective length of the laser cavity. This in turn shifts the locations of the resonances.

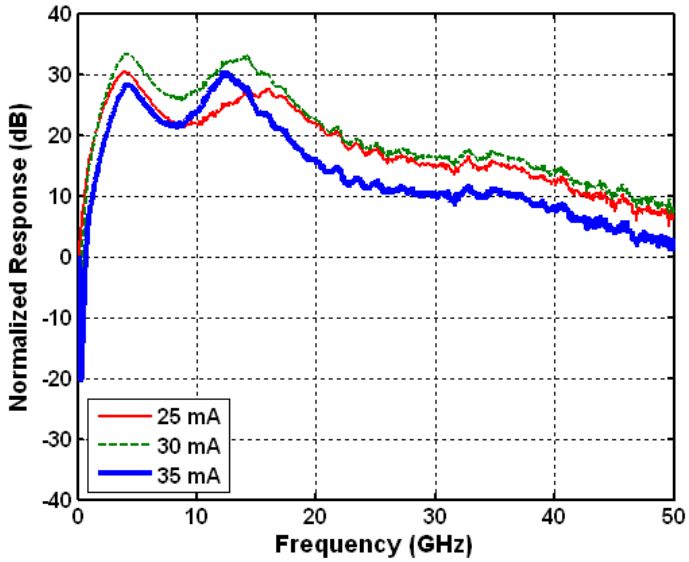

Figure 13: Small signal frequency response of the coupled cavity device for varying slave laser gain current. ($I_{master\ gain}$ = 70 mA, V_{EAM} = -2V)

We have also measured the frequency response for varying slave laser gain biases (Figure 13). In this case, there is not a direct connection between the increase in photon density and the amplitude of the second resonance. This is because the photon density in both laser cavities is dominated by the light generated in the gain section of the master laser. The resonance amplitude increase with increasing bias due to the movement of the operating position within the lock-band. At 35 mA bias current in the slave laser, the lasers are operating closer to the edge of the lock-band than at 25 mA, which results in a larger resonance, as previously shown with discrete devices [9].

3.3.3 55% Mirror Reflectivity Design

The PIC with stronger coupling between the lasers is designed for 99%, 55%, 55% and 90% reflectivities for the master rear mirror, master front mirror, slave rear mirror and slave front mirror respectively. In this case, the master laser consists of a 150 µm long rear mirror, 50 µm long phase section, 500 µm long gain section and 30 µm long front mirror. The slave laser consists of a 30 µm long rear mirror, 50 µm long phase section, 200 µm long gain section and 58 µm long front mirror.

As with the other designs, single frequency operation indicates the lasers are operating in the mutually injection locked regime. An optical spectrum from the injection locked lasers with greater than 35 dB side mode suppression ratio is shown in Figure 14.

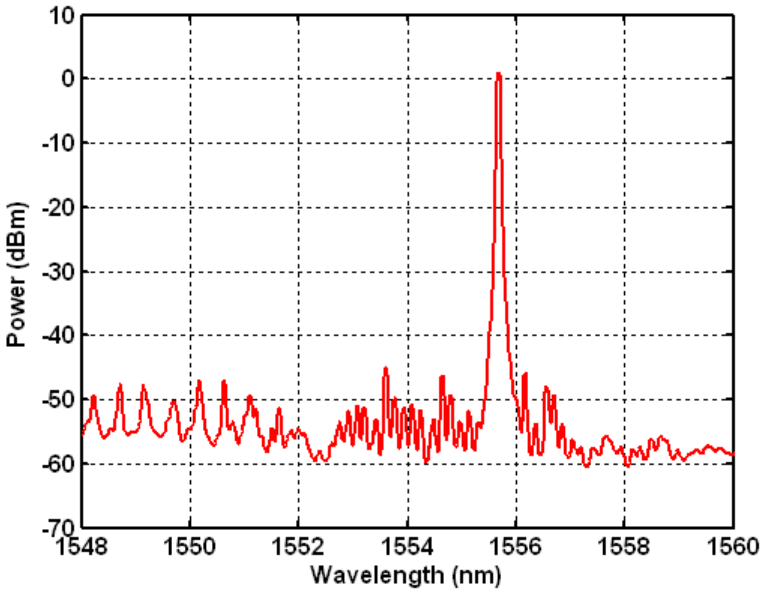

Figure 14: Optical spectrum of the PIC. ($I_{gain\text{-}slave}$ = 35 mA, $I_{gain\text{-}master}$ = 72 mA, V_{EAM} = -1.5 V).

The bandwidth of the device was measured using a 50 GHz network analyzer. The output from the network analyzer drives the EAM. A 50 Ω load resistor on the probe was placed in parallel with the EAM for impedance matching. The two laser gain sections were biased with a constant current. Applying current to the phase and mirror sections allows tuning of the relative cavity lengths and mode spacing. Biases were optimized to obtain single mode operation, which indicates mutual injection locking of the master and slave lasers. The only inputs to the chip were DC electrical biases and the electrical modulation signal. The device output was coupled into a lensed fiber and detected by a high-speed photodetector connected to the input of the network analyzer. The bandwidth of the EAM by itself was taken as a reference from a separate device consisting of a DBR laser and EAM of the same design. To ensure that the modulated power was similar, the laser on the EML chip was biased to achieve the same photocurrent as the injection locked PIC. The direct modulation bandwidth of the slave laser was taken with a 4 V reverse bias on the EAM to suppress feedback from the master laser cavity.

The small signal responses are seen in Figure 15. The complete PIC with the EAM under modulation has a bandwidth extending beyond the 50 GHz measurement capabilities of the network analyzer. This is a considerable improvement over the 10 GHz and 2.5 GHz bandwidths demonstrated by the integrated DBR-EAM and directly modulated slave laser respectively. It has been shown that the modulation sideband interaction with the free running laser cavity modes is responsible for the resonance frequency enhancements [12]. Since there are no isolators involved in the device, the PIC consists of five coupled active laser cavities leading to closely spaced cavity mode spacing. These closely spaced modes create the multiple response enhancements seen in the plotted frequency response. The plotted frequency response is not normalized and the same output modulation power level was used for all testing. Therefore, the relative amplitudes of the frequency response show that the injection-locked PIC has a higher modulation efficiency compared to the EAM alone. Increasing the cavity photon density, through higher gain currents, would dampen the frequency enhancements creating a flat

response, however this device did not achieve single frequency operation in this regime due to the designs cavity mode spacing and coupling strength.

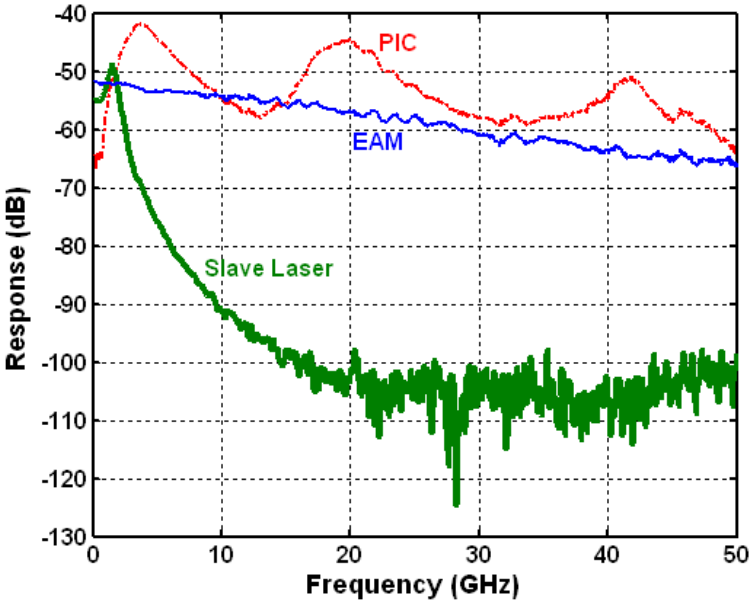

Figure 15: Small signal frequency response of the PIC ($I_{gain\text{-}slave}$ = 35 mA, $I_{gain\ master}$ = 72 mA, V_{EAM} = -1.5 V), slave laser ($I_{gain\text{-}slave}$ = 35 mA), and DBR-EAM (V_{EAM} = -1.5 V).

3.3.4 Summary of Mutually Injection Locked PICs with EAMs

In summary, a PIC with two DBR lasers and an EAM has been fabricated. Mutual injection locking between the two lasers has been demonstrated and the lock-band measured. The frequency response measurements show a five-fold increase in the device bandwidth compared to the EAM by itself. These PICs have demonstrated injection locking dynamics similar to large complex tabletop systems employing discrete lasers and isolators. The simplicity and compatibility with integration of the PIC make it an attractive building block in highly-functional PICs. These devices would be well suited for applications requiring a narrow frequency range at high frequencies. It is expected that improved engineering of the cavity spacing and coupling strengths will produce devices with the broadband response needed for many applications.

4. CONCLUSIONS

We have been successful in simulating and experimentally demonstrating that the modulation response enhancement from optical injection locking is possible even if the optical isolator between the master and slave lasers is removed. This was done through the development of composite coupled-mode theory capable of treating strongly coupled lasers and providing a rigorous description of outcoupling. This modeling provided a greater fundamental understanding of the physical mechanisms of the modulation of devices under injection locking. The characterization of PICs designed according to the simulations verified the modulation enhancement attributed to optical injection locking in coupled-cavity devices. Additionally, more complex PICs incorporating an EAM demonstrated this enhancement without a low frequency roll off. Ultimately, we have demonstrated PICs with strongly coupled-cavities that have resonance frequencies tenfold that of a directly modulated laser and bandwidths 5x that of a laser-modulator pair. A significant increase in the modulation efficiency under mutual injection was also shown. Due to their compact size, these devices have to potential to be important components of integrated photonics microsystems requiring extremely high bandwidths.

4. REFERENCES

1. L. Chrostowski, X. Zhao, and C.J. Chang-Hasnain, "Microwave Performance of Optically Injection-Locked VCSELs," IEEE Trans. on Microwave Theory and Techniques, Vol. 54, No. 2, pp. 788-796, 2006
2. W.W. Chow, "Theory of emission from an active photonic lattice," Phys. Rev. A, Vol. 73, No. 1, pp. 013821-1-013821-9, 2006
3. W.W. Chow, Z.S. Yang, G.A. Vawter, and E.J. Skogen, "Modulation Response Improvement With Isolator-Free Injection-Locking," IEEE Photonics Tech. Letters, Vol. 21, No. 13, pp. 839-841, 2009
4. W.W. Chow, "Dynamics in Isolator-Free Injection-Locked Lasers," IEEE/LEOS Winter Topicals Meeting Series, Innsbruck, Jan. 12-14, 2009
5. W.W. Chow, E.J. Skogen, and G.A. Vawter, "Modulation Response in Isolator-Free MOPA and Injection-Locked Laser Configurations," IEEE Int. Semiconductor Laser Conference, Sorrento, Sept. 14-18, 2008
6. A. Tauke-Pedretti, G.A. Vawter, E.J. Skogen, G. Peake, M. Overberg, C. Alford, W.W. Chow, Z.S. Yang, D. Torres, and F. Cajas, "Frequency Response Enhancement in Integrated Coupled-Cavity DBR Lasers", Photonics Society Annual Meeting, Denver, Nov. 7-11, 2010
7. A. Tauke-Pedretti, G.A. Vawter, E.J. Skogen, G Peake, M. Overberg, C. Alford, W.W. Chow, Z.S. Yang, D. Torres, and F. Cajas, "Mutually Injection-Locked Lasers Integrated with an Electro-absorption Modulator", submitted to Optics Letters.
8. E.J. Skogen, J.S. Barton, S.P. DenBaars, and L.A. Coldren, "A Quantum-Well-Intermixing Process for Wavelength-Agile Photonic Integrated Circuits," IEEE Journal of Sel. Topics in Quantum Electronics, Vol. 8, No. 4, pp. 863-869, 2002
9. E.K. Lau, H.-K. Sung, and M.C. Wu, "Frequency Response Enhancement of Optical Injection-Locked Lasers," IEEE J. of Quantum Electronics, Vol. 44, No. 1, pp. 90-99, 2008
10. H.-K. Sung, T. Jung, M.C. Wu, D. Tishinin, T. Tanbun-Ek, K.Y. Liou, W.T. Tsang, "Modulation Bandwidth Enhancement and Nonlinear Distortion Suppression in Directly Modulated Monolithic Injection-locked DFB Lasers," International Topical Meeting on Microwave Photonics, pp. 27-30, 2003
11. E.K. Lau, L.J. Wong, X. Zhao, Y.-K. Chen, C.J. Chang-Hasnain, M.C. Wu, "Bandwidth Enhancement by Master Modulation of Optical Injection-Locked Lasers," J. of Lightwave Technology, Vol. 26, pp. 2584-2593, 2008
12. X. Zhao, D. Parekh, E. K. Lau, H. K. Sung, M. C. Wu, W. Hofmann, M.C. Amann and C. J. Chang-Hasnain, "Novel cascaded injection-locked 1.55-μm VCSELs with 66 GHz modulation bandwidth," Optics Express, Vol. 15, pp. 14812-14816, 2007

DISTRIBUTION

1	MS1078	Wahid Hermina	1710
1	MS1082	Joel Wendt	1725
1	MS1085	G. Allen Vawter	1742
1	MS1085	Erik Skogen	1742
1	MS1085	Anna Tauke-Pedretti	1742
1	MS1085	Mark Overberg	1742
1	MS1085	Gregory Peake	1742
1	MS1085	Charles Sullivan	1742
1	MS1086	Weng Chow	1123
1	MS0899	Technical Library	9536 (electronic copy)
1	MS0123	D. Chavez, LDRD Office	1011


Sandia National Laboratories